Stable Multimetallic Nanoparticles for Oxygen Electrocatalysis

Steven D. Lacey, †, Lo Qi Dong, Lo, Zhennan Huang, Jingru Luo, Hua Xie, Zhiwei Lin, Dylan J. Kirsch, Vivek Vattipalli, Christopher Povinelli, Wei Fan, Reza Shahbazian-Yassar, Dunwei Wang,*,‡ and Liangbing Hu*,†®

Supporting Information

ABSTRACT: Nanostructured catalysts often face an important challenge: poor stability. Many factors contribute to catalytic degradation, including parasitic chemical reactions, phase separation, agglomeration, and dissolution, leading to activity loss especially during long-term catalytic reactions. This challenge is shared by a new family of catalysts, multimetallic nanoparticles, which have emerged owing to their broad tunability and high activity. While significant synthesis-based advances have been made, the stability of these nanostructured catalysts, especially during catalytic reactions, has not been well addressed. In this study, we reveal the critical influence of a synthetic method on the stability of nanostructured catalysts through aprotic oxygen catalysis (Li-O₂ battery) demonstrations. In comparison to the conventional wet impregnation



(WI) method, we show that the carbothermal shock (CTS) method dramatically improves the overall structural and chemical stability of the catalyst with the same elemental compositions. For multimetallic compositions (4- and 8-elements), the overall stability of the electrocatalysts as well as the battery lifetime can be further improved by incorporating additional noncatalytically active elements into the individual nanoparticles via CTS. The results offer a new synthetic path toward the stabilization of nanostructured catalysts, where additional reaction schemes beyond oxygen electrocatalysis are foreseeable.

KEYWORDS: Stability, heterogeneous catalysts, multicomponent metallic nanoparticles, carbothermal shock, Li-O₂ batteries

he instability of nanostructured heterogeneous catalysts, for example, nanoparticles, ¹⁻⁴ nanoclusters, ^{5,6} and atomically dispersed active sites, ⁷⁻⁹ is commonly observed in a variety of reactions. It is well-known that oxidative dissolution and agglomeration of Pt on carbon supports readily occur during the oxygen reduction reaction (ORR) in polymer electrolyte membrane fuel cells. For the hydrogen evolution reaction (HER) and CO2 reduction reactions, the detachment and migration of catalysts also transpire frequently, 14-16 particularly under high reaction rates where gaseous products are quickly converted at the solid/liquid interface. Such problems often become more pronounced when further downsizing the catalytic unit. For example, similar to the aforementioned cases, previous studies have shown that the chemical and structural stability of nanocluster catalysts were rarely ideal during long-term oxygen evolution reactions (OER) in which a multiphase environment is involved. ^{17,18} Similar issues arise when nanoclusters are exposed to aprotic environments ^{19,20} or undergo hightemperature gas-phase reactions.^{21,22} Recently, there has

been a growing interest in atomically dispersed active sites and subnanometer-scale clusters for catalytic applications; however, even short-term stability of these anchored species presents a formidable challenge. 23,24

To improve the stability of nanostructured heterogeneous catalysts, significant efforts have been made in terms of optimizing the substrate to enhance interfacial binding^{25,26} as well as in the modification of the catalyst to preserve the desired morphology and valence. 27,28 Nevertheless, how to maintain long-term stability of the supported catalyst while balancing the desired catalytic activity remains an urgent quest to be fulfilled by the community. Such a problem is shared with an increasingly important class of catalysts: multimetallic nanoparticles. Typically, multimetallic nanoparticles are synthesized by wet chemistry methods, namely wet impregna-

Received: April 13, 2019 Revised: July 2, 2019 Published: July 17, 2019

[†]Department of Materials Science and Engineering, University of Maryland, College Park, Maryland 20742, United States

[‡]Department of Chemistry, Boston College, Chestnut Hill, Massachusetts 02467, United States

[§]Department of Mechanical and Industrial Engineering, University of Illinois at Chicago (UIC), Chicago, Illinois 60607, United

Department of Chemical Engineering, University of Massachusetts, Amherst, Massachusetts 01003, United States

tion (WI), that feature a delicate balance among different processing parameters (precursor concentration, reducing agents, reaction temperatures, coordination ligand types/ concentrations, among others) to achieve the optimal properties.^{29–33} However, since different elements feature drastically different physicochemical properties, slight parameter changes of the aforementioned processes could result in detrimental effects to the synthesized multielemental nanoparticles.³⁴ Moreover, catalytic operations can further exacerbate the decomposition (such as phase separation, agglomeration, and detachment) of multimetallic nanoparticles, which leads to poor catalytic activity and short catalyst lifetime. While active research efforts aim to establish effective protocols for the systematic and reliable production of stable multimetallic nanoparticles using solution-based methods^{35–37} and beyond (e.g., lithography), ^{38–40} the issue of catalyst stability, especially for long-term operation, still persists.

As one of the most important energy storage systems that necessitates catalysts, aprotic Li-O2 batteries received significant attention in the past two decades by promising the highest theoretical energy density due to the cathode's surface-based conversion chemistry. 41-44 Applying efficient cathode electrocatalysts have shown success in facilitating ORR during discharge and, particularly, OER during recharge. 45-However, long-term stability of the current catalytic candidates remains a critical issue, especially when operating under harsh testing conditions. ^{47,48} The Li-O₂ cathode operates within a rather delicate system that involves solid/liquid/gas interfaces during ORR and OER. 41-43,48 Severe parasitic reactions are well documented, which further reduces the catalyst's overall stability. 48-50 With repeated formation and decomposition of lithium peroxide (Li_2O_2) as well as other reactive byproducts, the catalysts are prone to degradation, detachment, agglomeration, and/or elemental segregation. 42,49,51 For practical applications, battery operations usually require months of reliable performance with frequent switching of polarities between discharge and recharge, necessitating good stability of the catalysts and highlighting the gap between the needs and what can be provided by existing materials.⁵² Using aprotic Li-O₂ batteries as a model system, we evaluate catalysts prepared by different synthesis methods in order to reveal critical factors that influence catalytic stability and, consequently, overall electrochemical performance. In comparison to conventional wet chemistry approaches (such as WI), we previously showed that the carbothermal shock (CTS) method enables exploration of more complex multimetallic nanoparticle compositions (up to 8-element) due to significant temporal restrictions (i.e., synthesis duration of milliseconds to seconds).⁵³ In the current work, not only are improvements in multimetallic particle size reported but also the topic of catalyst stability induced by the CTS synthesis method is highlighted for the first time. Together with enhanced structural and chemical stability, these supported nanocatalysts synthesized by CTS facilitate superior long-term electrocatalytic operation compared to WI, as evidenced by the extended cycle life of the reported Li-O₂ batteries. We envision that the synthetically induced stability reported herein is applicable to other catalytic systems (beyond oxygen electrocatalysis) that require stable supported catalysts, such as fuel cells, water splitting, and hydrocarbon conversion devices.

Results and Discussion. To evaluate the influence of synthesis method on the stability behavior of the catalysts, a suitable cathode substrate (i.e., catalyst support) and an

efficient catalyst for oxygen electrocatalysis were first identified. Carbon-based materials are predominantly used by the Li-O₂ research community as both the cathode and catalyst support. 54-56 Despite the potential complications due to parasitic reactions of carbon against reactive oxygen species during long-term operation, 48,49 it offers advantages such as low cost, good ORR activity, and high surface area that are critical for high capacities. 42,54,57 Moreover, carbon is the most widely used and studied substrate material for many other reaction systems, where a variety of carbon materials have been developed through synthetic approaches, with some being commercialized and massively produced (e.g., Vulcan carbon black).⁵⁸ For Li-O₂ battery operation, a tunable and wellcontrolled porous structure would be ideal both to accommodate the reaction products and to investigate the reaction mechanisms. 59,60 Three-dimensionally ordered mesoporous (3DOm) carbon was, therefore, chosen for this body of research. It features a high surface area (ca. 1200 m² g⁻¹) and tunable mesoporosity, where interconnected spherical pores are formed during the colloidal crystal templating process.⁵⁹ 3DOm carbon also features a variety of surface functional groups (particularly carboxylic, lactonic, and phenolic), 61 which serve as nucleation sites for metal precursors to adsorb onto and anchor sites for the synthesized nanocatalysts (Figures S1-S3). Most importantly, unlike other carbon substrates whose overall structural uniformity and regularity are difficult to control, the highly ordered and well-defined structure of 3DOm carbon permits detailed mechanistic studies on the various factors that may contribute to the stability issues, such as particle agglomeration or detachment.

Next, we evaluated which catalysts were suitable for this study. From the literature, ruthenium (Ru)-based catalysts appear to be one of the best for Li-O₂ battery operation. ^{62,63} Our previous study as well as those by others have shown that Ru-based catalysts exhibit superior OER activity and suitable ORR activity. 63-65 Similarly, iridium (Ir) has been reported effective in facilitating discharge and recharge processes during Li-O₂ battery operation.⁶⁶ In particular, the use of Ir has been shown to achieve one of the highest Li₂O₂ yields, resulting in appreciably lower parasitic reactions.⁶⁷ We were, thus, guided to build an alloy system around these two elements while keeping in mind the potential concerns, including high cost. Consequently, material cost led to both the exploration and incorporation of inexpensive transition-metal elements, which have been reported to exhibit limited activity toward ORR and OER in aprotic environments. 46,47 Thus, Ru-rich catalytic systems combined with Ir (namely, 3:1 Ru:Ir) as well as noncatalytic metallic components are chosen for this study to achieve both binary and multimetallic nanoparticle compositions. In the literature, multimetallic catalysts have also been prepared by wet chemistry methods (such as WI) in either a well-mixed (i.e., solid solution) or phase-separated state based on the thermodynamically favorable phase and specific elemental combination. 30,68 In stark contrast to the conventional WI method, CTS is capable of forming highly dispersed nanoparticles with beyond trimetallic compositions (up to 8 elements), independent of elemental immiscibility⁵³ (Figure 1). Nanoscale catalysts with such elemental richness and dispersity, as shown in Figure 1, are rare in the literature. The temporal limitations inherent to the rapid and tunable CTS process lead to unique synthetic capabilities as well as exceptional control in terms of sample morphology, where well-dispersed and ultrasmall nanoparticle sizes are readily

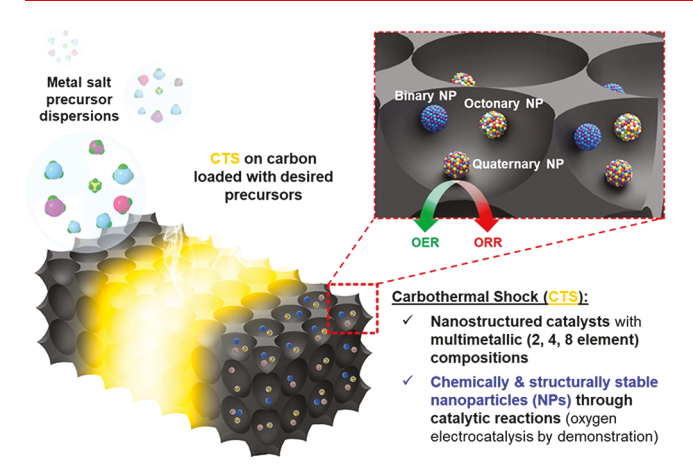


Figure 1. Schematic representation of the process and capabilities of the CTS synthesis method. Nanostructured catalysts with multimetallic compositions are readily achievable via CTS on carbon supports, which exhibit enhanced structural and chemical stability compared to conventionally synthesized nanocatalysts.

achieved due to short heating/quenching time scales (on the order of milliseconds to seconds). Thus, the CTS method produces non-agglomerated nanoparticles with optimum control over particle size, structure, and elemental composition, which are promising attributes that could lead to improved catalytic stability over nanoparticles fabricated by conventional synthesis methods with slow reduction steps.

In a typical synthesis process, CTS was achieved by electrically triggered Joule heating of the precursor-loaded carbon supports in an Ar-filled glovebox (Figure 2a-c). Figure 2a shows the typical morphology of the 3DOm carbon 69 before precursor loading. The bare 3DOm carbon was then loaded dropwise with the desired (Ru and Ir) precursor salts in solution and undergoes brief exposure to high temperature due to the applied high current electrical pulse (Figure 2b). After CTS, nanosized particles evenly decorated the carbon substrate, while the ordered 3DOm structure (i.e., templated carbon replica) was preserved, as shown in Figure 2c and Figure S4. It is important to note that while Ru and Ir each

exhibits good catalytic activity as measured by low overpotentials, the combination of the two via CTS, in varying ratios, offers even better electrochemical performance (Figures S5 and S6). Notably, ratios from Ir-rich to Ru-rich (1:3 to 12:1) all exhibited similar overpotentials and terminal potentials, as shown in Figure S6. The morphology and level of particle dispersion were highly reproducible between different samples and apparent throughout the 3DOm's interconnected mesopores. The size and dispersion of the CTS-synthesized bimetallic 3:1 Ru:Ir nanoparticles on 3DOm are shown more clearly by high-resolution imaging (Figure 2d). The prepared RuIr nanoparticles were predominantly 2-3 nm in diameter, evenly dispersed across the defective sites of the 3DOm carbon support, and crystalline in nature (Figure 2d with inset). Since the loaded 3DOm carbon support was exposed to high temperature for a short time (≤ 1 s), it provides temporal limitations to prevent nanoparticle agglomeration and coarsening that typically occurs with extended synthesis durations found in conventional methods (e.g., hours of reaction in furnaces). Consequently, a narrow particle size distribution and homogeneous mixing of elements (e.g., Ru and Ir) were achieved by the rapid CTS process, as shown in Figure 2e-f. The same CTS process could be readily transferred to other carbon substrates such as on commercial Vulcan carbon black (Figure S7) or even carbon nanofibers, as previously reported by our lab.⁵³ Due to its limited surface area, however, relatively poor battery performance was measured on Vulcan carbon compared to 3DOm carbon supports with identical CTS electrocatalyst compositions (Figure S8). This disparity in catalytic performance can be attributed to the better morphological control enabled by 3DOm carbon. 59 The results further highlight the uniqueness of the 3DOm carbon as a study platform with the ease of monitoring potential morphological or compositional changes on a substrate with well-defined structures.

To determine the effect of the synthesis methods (CTS vs WI) on nanoparticle formation and stability, we synthesized RuIr bimetallic nanoparticles via CTS and the conventional WI method, where identical metal salt precursors (3:1 Ru:Ir) and 3DOm supports were employed; however, the latter relies on a relatively slow thermal reduction process in a tube furnace in

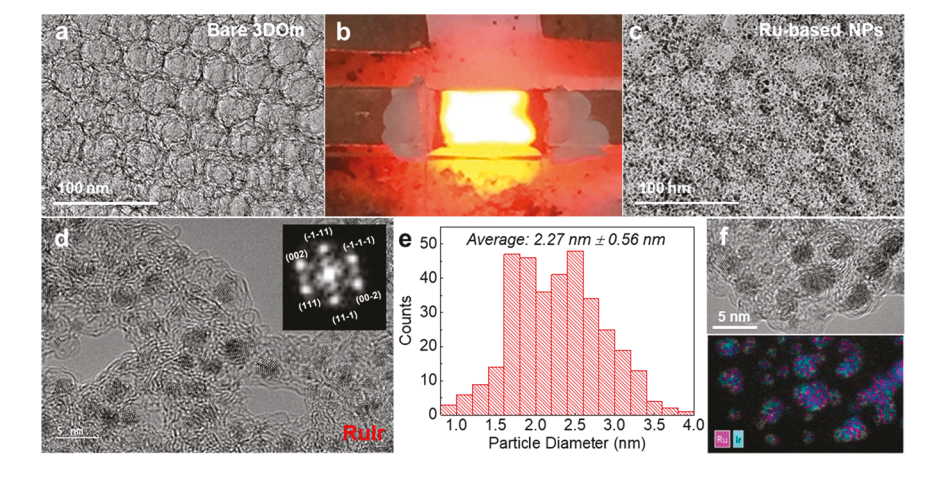


Figure 2. Synthesis and characterization of CTS-synthesized Ru-rich electrocatalysts. (a) Bare 3DOm carbon support used to load multiple metal salt precursors. (b) Precursor-loaded 3DOm film emitting light during the electrically triggered CTS process. (c) Ru-rich multimetallic nanoclusters uniformly decorating the 3DOm support, where the 3DOm structure is retained after <1 s exposure to high temperature. (d) HRTEM image of bimetallic RuIr nanoparticles, which are evenly dispersed and crystalline in nature (see the inset FFT pattern with $[1\overline{1}0]$ zone axis). (e) Particle size and (f) elemental distribution of the 2–3 nm solid solution RuIr particles on 3DOm.

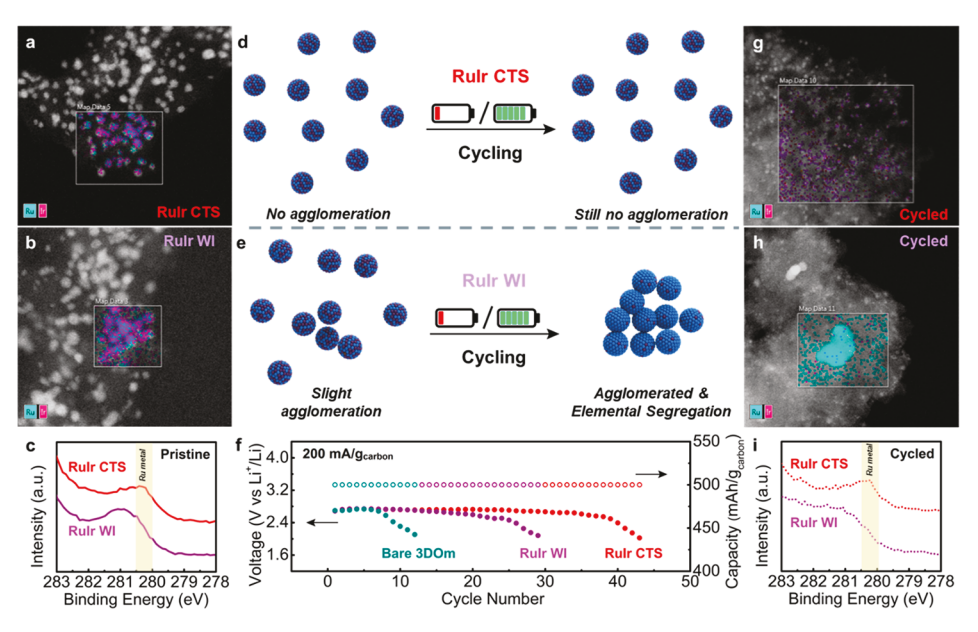


Figure 3. Nanoparticle stability comparison between the CTS and WI method. HAADF elemental maps of RuIr-loaded 3DOm fabricated by (a) CTS and (b) the conventional WI methods. (c) XPS Ru 3d spectra of the as-prepared cathodes by the respective CTS and WI methods. Compared to CTS, the nanoparticles prepared by the WI method were already oxidized and not as well distributed across the 3DOm surface, where slight agglomeration was present. The yellow shaded region corresponds to the binding energy of Ru metal. (d, e) Schematics showcasing the disparate stability between CTS- and WI-synthesized RuIr nanoparticles before and after aprotic Li-O₂ battery operation. (f) Cycling performance (tested at 200 mA g_{carbon}^{-1} or 0.2 mA cm⁻²) that compares the bimetallic Li-O₂ battery cathodes via CTS and WI to bare 3DOm, where the trends correspond to reproducible data sets. The *y*-axis dictates the terminal voltage upon discharge in each cycle, which showcases the cycling stability. The STEM-EDS elemental maps of the cycled Li-O₂ battery cathodes prepared by (g) CTS and (h) WI with corresponding (i) XPS Ru 3d spectra. After electrochemical cycling, the CTS-synthesized nanoparticles remain (chemically, structurally) stable, while severe elemental segregation and particle agglomeration plague the WI nanoparticles, which limits the catalyst's overall stability and results in the greatly reduced cycle life shown in (f). Note the yellow shaded regions in (c) and (i) correspond to the binding energy of metallic Ru.

order to transform the precursors into nanostructured catalysts. Figure 3a,b compares the as-synthesized nanoparticles by CTS and WI methods in terms of size, shape, dispersion, and elemental distribution through high-angle annular dark-field (HAADF) images and elemental maps. Despite slight particle agglomeration, the RuIr catalysts synthesized by the WI method are identical to the CTS nanoparticles in terms of size (few nanometers in diameter) and shape. Additionally, the elemental components (Ru, Ir) within the WI-synthesized nanocatalysts are also uniformly mixed, similar to the CTS nanoparticles. Since the initial metal precursor ratio/loading, nanoparticle size/shape, and elemental distribution of the CTS and WI nanoparticles are common features, the two nanoparticle systems can be directly compared in terms of overall catalyst stability. However, the initial difference between the CTS and WI nanoparticles is evident from the microscopy images, where slight agglomeration is present for the WI method. Two potential reasons for the agglomerates are as follows and are directly linked to the slow thermal reduction procedure: (1) The defect density and surface groups on the 3DOm carbon are changed due to prolonged exposure at high temperature, which limits the amount of anchor sites during the WI process; and (2) the long time scales at high temperature cause particle coarsening and agglomerates readily form. In order to rule out changes to the carbon support during the WI method's slow thermal reduction step, bare 3DOm carbon supports were exposed to an identical furnace treatment without precursor loading and then subjected to the rapid CTS process after loading identical metal salt precursors (ratio of 3:1 Ru:Ir). The defect level (i.e., $I_{\rm D}/I_{\rm G}$ ratio) of the 3DOm carbon supports before and after

conventional heat treatment in a tube furnace was identified via Raman spectroscopy (Figure S9). Notably, the defect level between the samples is nearly identical ($I_{\rm D}/I_{\rm G}\sim 0.95$ for bare 3DOm and 0.93 for furnace treated 3DOm), which indicates that the carbon support does not undergo changes during the furnace heat treatment. Additionally, TEM images and XPS spectra showed no obvious changes in terms of particle size/dispersion or chemical composition between the bare and furnace treated 3DOm carbon (Figures S10 and S11). Therefore, the slight particle agglomeration observed for the WI-synthesized nanoparticles arises from exposure of the precursor-loaded supports to high temperature for prolonged time scales.

The chemical composition of the CTS- and WI-synthesized nanocatalysts was explored via an additional spectroscopy technique. Specifically, X-ray photoelectron spectroscopy (XPS) revealed that the nanoparticle's major elemental component, Ru, is metallic in nature (as shown by the yellow shaded region) after CTS synthesis, whereas the Ru-rich WI nanoparticles were oxidized. This was evident by the shift to higher binding energies in the Ru 3d XPS spectra for the WI catalysts, which corresponds to a change in oxidation state to Ru⁴⁺ due to the formation of RuO₂ (Figure 3c). By design (i.e., metal precursor loading), both synthetic methods were expected to form bimetallic alloy nanoparticles since CTS occurs in an Ar-filled glovebox and WI occurs in a tube furnace with a constant Ar flow; however, the formation of (ruthenium) oxides instead of metals/alloys has been prevalent for wet chemistry approaches as reported in the literature. 63,65,70 The use of a glovebox with very low ppm levels of oxygen and water (which is likely much smaller than levels

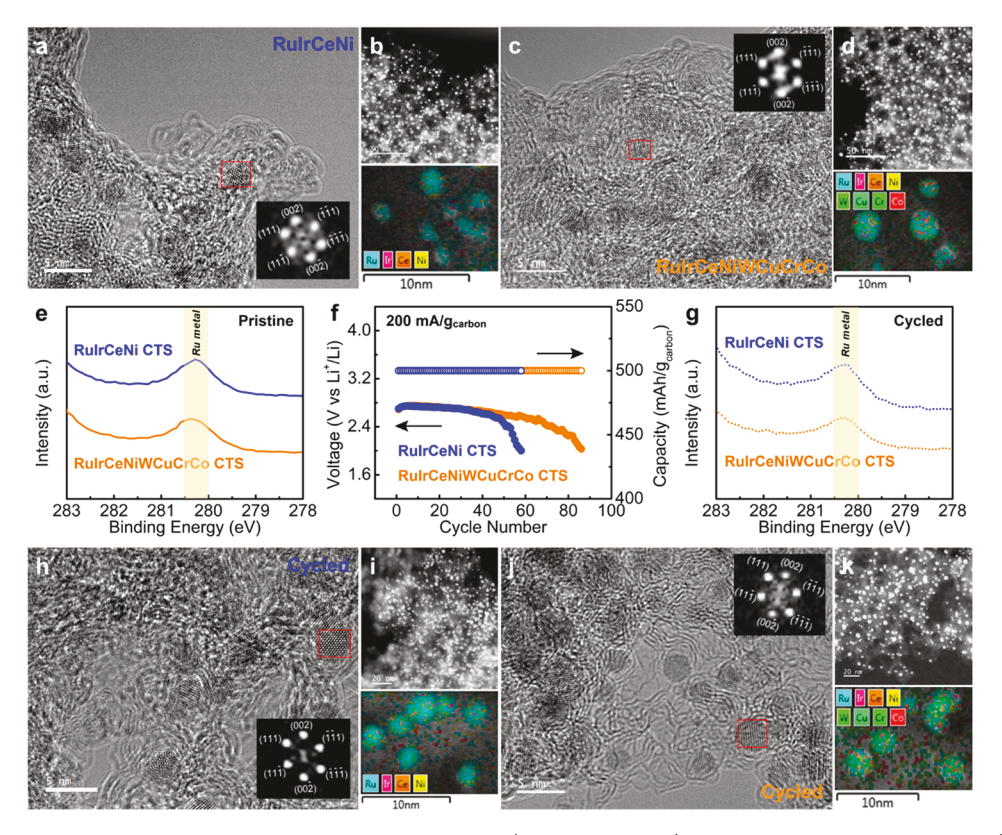


Figure 4. Characterization and stability of CTS-synthesized multimetallic (4- and 8-element) nanoparticles on 3DOm carbon. (a, c) HRTEM and (b, d) STEM-HAADF images with elemental overlay maps of the as-prepared RuIrCeNi and RuIrCeNiWCuCrCo nanoparticles via CTS, respectively. (e) XPS Ru 3d spectra for both multimetallic nanoparticle compositions directly after synthesis. (f) Long-term Li-O₂ battery demonstration of the CTS-synthesized RuIrCeNi (blue curve) and RuIrCeNiWCuCrCo (orange curve) 3DOm cathodes. Note that the *y*-axis is the terminal voltage upon discharge for each cycle. (g) XPS Ru 3d spectra for the 4- and 8-element nanoparticle compositions, which remain metallic in nature (yellow shaded region) even after electrochemical cycling. Post-analysis (h, j) HRTEM and (i, k) STEM-HAADF images with elemental overlay maps of the cycled RuIrCeNi and RuIrCeNiWCuCrCo nanoparticle-decorated 3DOm upon Li-O₂ battery operation, respectively. Both CTS-synthesized 4- and 8-element nanoparticles remain well-dispersed on the 3DOm carbon and exhibit exceptional structural and chemical stability after Li-O₂ battery operation. Note that each inset FFT pattern, which was taken from the areas boxed in red (a, c, h, j) and has a [110] zone axis, verifies the crystallinity of the aforementioned nanoparticles prepared by CTS both before and after electrochemical cycling.

in a tube furnace) may be responsible for the lower oxidation state (i.e., metallic nature) of the CTS-synthesized RuIr nanoparticles. This understanding has prompted us to propose another possible reason for the slight agglomeration observed for the as-prepared WI nanoparticles (Figure 3b), which is due to surface energy differences between these oxides and the CTS-synthesized alloy nanoparticles.

To evaluate the catalytic activity and stability between CTS and WI nanoparticles, the as-prepared RuIr-based electrocatalysts on 3DOm carbon were electrochemically cycled within a Li-O₂ configuration. Since the physical attributes of the as-prepared electrocatalysts by CTS and WI were identical, we did not expect significant variations in the catalytic activity toward ORR/OER. Indeed, a nearly similar ORR and OER activity was observed during a single discharge and recharge cycle at a current density of 200 mA g_{carbon}^{-1} even though the overpotential of the CTS sample is slightly lower than the WI (Figure S12). Only when the current density was increased to 500 mA g_{carbon}⁻¹ did the CTS bimetallic nanoparticles show noticeably better catalytic activity. It is important to note that single cycle characterization, as shown in Figure S12, mainly highlights the intended "catalytic" activity of the nanoparticles as measured by the overpotentials. Another key functionality of the catalyst, to promote intended chemical reactions and to minimize parasitic reactions, is best tested by cyclability. In this

case, performance differences are likely attributed to catalyst agglomeration and decomposition, which would lead to cell failures over time due to the accumulation of inactive Li₂O₂ and other byproducts such as organic carbonates. 46-48,51 This mechanism is schematically represented in Figure 3d,e for catalysts synthesized by each synthetic technique (CTS, WI). Indeed, a drastic difference in cycle life was observed between catalysts synthesized by CTS and WI. As shown in Figure 3f, the cell with CTS-synthesized electrocatalysts (43 cycles) outlasted the WI-synthesized ones (29 cycles) with ca. 48% improvement in cycle life under the same testing conditions. Note that the observed trend was repeated for each composition at least three times. Without the presence of catalysts, the bare 3DOm carbon cathode lasted only 13 cycles under the same testing conditions with poor voltage stability (Figure 3f).

To understand why the synthetic methods produce electrocatalysts with significantly variant cyclability, various microscopy and spectroscopy techniques were employed to characterize each Li-O₂ battery cathode after 20 cycles of discharge/recharge (Figure 3a-c). As can be seen from the HAADF images and corresponding elemental mapping, the morphology and elemental distribution of the cycled electrocatalysts synthesized by CTS and WI differed greatly (Figure 3g,h). The CTS-synthesized nanoparticles remained dispersed

on the 3DOm surface without obvious agglomeration or signs of elemental segregation (Figure 3g). However, the catalysts prepared by WI exhibited severe particle agglomeration and element segregation upon cycling (Figure 3h). Specifically, the WI-nanoparticles tended to form Ru-rich agglomerates on the order of tens of nanometers, which severely limited the performance of the cathode.⁴⁹ Note that the images shown in Figure 3g,h are indeed representative and reproducible over multiple samples/areas. Specifically, no noticeable particle agglomeration was ever observed for the electrochemically cycled CTS samples; however, the WI nanoparticles always became more agglomerated, although to different extents since the nanoparticles formed small agglomerates even before testing in Li-O₂ cells.

Chemical stability of the electrocatalyst upon cycling is another important aspect related to long-term Li-O2 battery operation. Notably, the Ru 3d spectra showed no change in the oxidation state for the cycled CTS cathode, whereas severe and continuous oxidation occurred for the WI cathode (Figure 3i). The resulted agglomeration and decomposition of the WI electrocatalyst reduced the overall density of active sites and catalytic activity of the cathode, eventually leading to decay in the Li-O₂ battery performance (Figure 3f). During electrochemical cycling, the high-energy surfaces of the chemically unstable WI nanoparticles facilitate the formation of agglomerates in order to reach a lower energy state. Unlike WI, the CTS electrocatalysts exhibited better chemical stability not only due to their high-entropy nature (i.e., solid solutions) but also from enhanced catalyst/substrate interactions since the brief (<1 s) synthesis preserves the surface defects on 3DOm. 33 This is a further indication that the synthetic method greatly influences the overall stability of the as-prepared catalysts both before and after electrochemical operation.

The extended capabilities of the CTS method arise when multiple elements are combined to form solid solution nanoparticles. In sharp contrast to the conventional WI method which is generally limited to up to three components within individual nanoparticles, the CTS method permitted the synthesis of electrocatalysts with significantly richer compositions (Figure 4a-d). Specifically, non-noble, catalytically inactive elements (e.g., Ni, Ce, among others) were added to the RuIr alloy (Figure S6). Figure 4a,b showed the uniform size and dispersion of RuIrCeNi nanoparticles fabricated on 3DOm carbon via CTS. These CTS-synthesized quaternary electrocatalysts were crystalline in nature (Figure 4a, inset) and similar to RuIr (Figures 2d-f and 3a) and ternary (RuIrNi) nanoparticles (Figures S13 and S14) fabricated using the CTS method in terms of particle size and dispersion, as well as elemental distribution (Figure S15). To further demonstrate elemental complexity, we introduced additional noncatalytic components (W, Cu, Cr, Co) into the quaternary composition to form octonary solid solution nanoparticles, while controlling the amount of Ru to ca. 76 at% in the final composition. The HRTEM and scanning transmission electron microscopy (STEM)-HAADF images shown in Figure 4c,d depict uniformly sized particles and distributions on the carbon support, while the overlay/individual maps (Figure 4d and Figure S16) provide strong evidence for the elemental distribution of these octonary nanoparticles composed of excess amounts of Ru and the existence of the other seven elements. It is important to note that both the CTSsynthesized quaternary (RuIrCeNi) and octonary (RuIrCe-NiWCuCrCo) compositions were metallic in nature, as

expected by design (Figure 4e). Through incorporation of these noncatalytically active elements (typically 3–4 at%), we expect minimal influences in terms of electrocatalytic performance, but more profound impacts on the catalyst's stability. Indeed, adding additional elements into the Ru-rich nanoparticles via CTS did not dramatically change the catalytic activity (and overpotential) for either 4- or 8-element compositions compared to the original bimetallic electrocatalyst (Figures S17 and S18).

Interestingly, while the catalytic activity remains comparable, the CTS quaternary and octonary electrocatalysts enabled their respective Li-O2 cells to reach 58 cycles and 86 cycles (Figure 4f). Intuitively, since the main catalytic component among all binary (CTS or WI), quaternary, and octonary nanoparticles is Ru and the same carbon support was employed for all electrochemical measurements, the reaction mechanism and associated discharge products should be nearly identical upon cycling for each 3DOm cathode regardless of nanoparticle composition. 42,71 Accordingly, there should be no obvious differences in product formation and detection between the cycled cathodes from scanning electron microscopy (SEM) and XPS post-analysis, which is confirmed in Figures S19–S21. Therefore, given that the test cells were identical in other components and the only difference was the cathode catalyst compositions, we were led to conclude the nature of the CTS electrocatalysts was the main reason for the enhanced cycling performance. The difference could be attributed to the following factors: (1) enhanced catalyst/substrate interactions due to the CTS method, where the short synthesis time (<1 s)aided nanoparticle anchoring to defective sites and prevented nanoparticle coarsening; (2) the incorporation of more catalytically inert elements into individual nanoparticles led to slight reductions in overall Ru content, which lessened parasitic chemical reactions inevitable to highly reactive Ru;⁴⁷⁻⁴⁹ and (3) nanoparticles composed of more elements (8-element vs 4- or 2-elements) featured higher configurational entropy (and, thus, lower Gibbs free energy), leading to enhancements in overall catalyst stability.5 Thus, the prolonged Li-O₂ cyclability shown in Figure 4f suggests improved chemical and structural stability of the CTSsynthesized multimetallic electrocatalysts.

To verify this hypothesis, various characterization techniques were employed on cycled quaternary and octonary nanoparticle-decorated 3DOm supports (Figure 4g-k). Figure 4g verified that the 4- and 8-element electrocatalysts retained their metallic nature without changes in oxidation states after repetitive Li-O2 operation. The results should be contrasted with those by WI-synthesized binary electrocatalysts, which suffered from significant oxidative degradation upon 20 electrochemical cycles. Beyond chemical stability, overall catalyst stability also depended on the nanoparticles' size, structure, and dispersity upon cycling. Compared to the original morphology, the particle size and elemental distribution of the 4- and 8-element compositions (Figure 4a-d and Figures S15 and S16), and the cycled samples showed no measurable differences (Figure 4h-k and Figures S22 and \$23). Specifically, both quaternary and octonary nanoparticles remained crystalline, 2-3 nm in diameter, and evenly distributed across the 3DOm surface without obvious signs of aggregation after electrochemical cycling. These results support the outstanding structural and chemical stability of the CTS-synthesized electrocatalysts in comparison to electrocatalyst compositions fabricated by conventional wet chemistry

approaches (such as WI). To extend the applicability of CTS catalysts toward other reaction schemes and avoid potential performance limitations associated with aprotic environments, the quaternary (RuIrCeNi) nanoparticle composition was also prepared on commercial Vulcan carbon and electrochemically tested using the water-in-salt electrolyte (WiS) platform^{72,7} (Figures S24 and S25). Previous studies have shown superior stability during Li-O2 battery operation using WiS electrolyte.⁷³ Compared to the previously reported cyclability with a bare Vulcan cathode (ca. 70 cycles), 73 a significant improvement in cell lifetime (250 cycles) and overpotential (reduced by a total of ca. 300 mV) was achieved using the CTSsynthesized quaternary electrocatalysts. Lastly, although not further exploited by this current study, the ability to include inexpensive transition metals also opened the door to reduce the overall cost of electrocatalysts whose active elements are noble metals.

Conclusion. In summary, we explored the overall stability of multimetallic catalysts (nanoparticles ca. 2-3 nm in diameters) supported on a substrate through electrocatalytic oxygen evolution and reduction reactions. Ru-rich solid solution nanoparticles in 2-, 4-, and 8-element compositions were fabricated on a mesoporous support (i.e., 3DOm carbon) by the rapid CTS method to determine the extent of nanoparticle agglomeration, elemental segregation, and catalytic stability before and after electrochemical cycling. Unlike nanoparticles fabricated using the conventional WI method, the CTS-synthesized nanoparticles exhibited significantly better particle dispersion and no obvious signs of agglomeration and elemental segregation before or after cycling in Li-O2 cells. To confirm that the enhanced catalyst stability arises from the CTS synthesis method and not from changes to the carbon support, a control experiment was performed, where bare 3DOm carbon was heat treated in a tube furnace using the WI method's same slow thermal reduction step and then loaded with identical metal salt precursors before applying CTS. The results verified the proposed claim that the difference in catalyst stability does not arise from the thermal treatment procedure altering the carbon's defect level or surface groups, but rather the prolonged time scales at high temperature enable the metal particles to coarsen and agglomerate during the WI process.

Additionally, unlike WI, more complex multimetallic nanoalloy compositions (>3 elements) are readily attained due to the inherent temporal restrictions of the CTS method (i.e., rapid heating to high temperature followed by quenching in milliseconds to seconds). The 8-element CTS electrocatalyst composed mainly of Ru with trace amounts of the other seven elements showed a much improved electrochemical performance, especially cycling stability. Due to the high Ru content and low percentage of predominantly noncatalytic elements (e.g., Ce, Ni), the overall catalytic activity of 4- and 8-element compositions toward ORR/OER was maintained, whereas the overall (structural and chemical) stability was enhanced due to the high configurational entropy of said nanoparticles and led to prolonged operation of the reported Li-O₂ battery cathodes. The chemical nature of the nanoparticles fabricated by CTS and WI also differed, where the former showed no signs of oxidation before or after electrochemical cycling, while the latter became oxidized directly upon synthesis and continually proceeded during Li-O₂ battery operation.

The superior stability (both structural and chemical) observed for CTS catalysts compared to WI leads to the

following two-part hypothesis: (1) the structural stability is inherent to the CTS synthesis method's rapid cooling step, and (2) the chemical stability is due to the high entropy nature of the synthesized nanoparticles. Specifically, the CTS method features ultrafast heating and, most importantly, ultrafast cooling, which freezes the highly dispersed solid solutions in the form of nanoparticles onto the substrate's defective sites. This leads to stronger binding with the substrate compared to the nanoparticle/substrate interactions present with the conventional WI method, where prolonged heating and cooling steps allow Ostwald ripening and particle migration to occur. However, the firmly anchored CTS catalysts are temporally locked into place and, thus, less prone to structural deformation, detachment, and/or aggregation. It is also possible that an additional chemical bond, such as M-C (M = metal; C = carbon), may be formed upon high-temperature heating between the metallic nanoparticles and the carbon substrate to further enhance structural stability, yet future research endeavors are needed to fully understand the chemical identity of the nanoparticle/substrate interface. In terms of chemical stability, the CTS catalysts are unique due to their high entropy. From a thermodynamic point of view ($\Delta G = \Delta H$ - $T\Delta S$), the high entropy nature $(\Delta S\uparrow)$ of the CTSsynthesized nanoparticles promotes improved thermodynamic stability $(\Delta G\downarrow)$ against reactive oxygen intermediates and electro-oxidation reactions. This hypothesis is supported by the stable oxidation states of the bimetallic, quaternary, and octonary nanoparticles during Li-O₂ battery operation. In contrast, WI-synthesized catalysts suffer from irreversible oxidative degradation. The hypothesis that higher entropy leads to better catalyst stability is also evidenced by the improved cyclability of the reported Li-O2 cells, where octonary compositions outperform quaternary, while quaternary exceed binary catalysts in long-term performance. On a system level, despite that no degradation was observed for all CTS catalyst compositions, we suspect that the catalyst with a more complex elemental composition (i.e., higher entropy) induces less side reactions toward other cell components such as the cathode and the electrolyte during Li-O2 battery operation. As a result, we hypothesize that the enhanced chemical, structural, and system-level stability of the reported CTS catalysts are due to the inherent features of this unique synthesis method. Note that the reported catalyst stability of CTS-synthesized nanoparticles should not be limited to oxygen electrocatalysis. Future studies are warranted in order to explore additional catalytic applications, such as in fuel cells, water splitting, hydrocarbon conversion, and other reaction schemes, where the (CTS) fabrication of highly dispersed and supported multimetallic nanoparticles with trace noncatalytic components could enhance overall device performance through improved catalyst/substrate interaction as well as structural and chemical stability.

ASSOCIATED CONTENT

S Supporting Information

The Supporting Information is available free of charge on the ACS Publications website at DOI: 10.1021/acs.nanolett.9b01523.

Details regarding the experimental methods; characterization of 3DOm carbon; voltage profiles of 1-, 2-, 3-, 4-, and 8-element Ru-based nanoparticle compositions (CTS and WI) on 3DOm; characterization and

electrochemical performance (both aprotic and water-insalt systems) of CTS-synthesized nanoparticles on commercial Vulcan carbon; control experiment to verify no changes occur on 3DOm carbon during furnace treatment; morphology and elemental maps of 4- and 8element CTS nanoparticles before and after electrochemical cycling; post-mortem characterization of cycled CTS and WI cathodes (PDF)

AUTHOR INFORMATION

Corresponding Authors

*E-mail: binghu@umd.edu. *E-mail: dunwei.wang@bc.edu.

ORCID ®

Steven D. Lacey: 0000-0003-1096-7699

Qi Dong: 0000-0002-7553-4213 Wei Fan: 0000-0002-8581-2651

Reza Shahbazian-Yassar: 0000-0002-7744-4780

Liangbing Hu: 0000-0002-9456-9315

Author Contributions

¹These authors contributed equally to this work.

Notes

The authors declare no competing financial interest.

■ ACKNOWLEDGMENTS

This study has no direct funding. S.D.L. acknowledges support by the Department of Defense through the National Defense Science and Engineering Graduate (NDSEG) Fellowship. Q.D. and J.L. were supported by the National Science Foundation (NSF) CBET 1804085. R.S.-Y. and Z.H.'s efforts and electron microscopy studies were supported by NSF-DMR award no. 1620901. This work made use of the JEOL JEM-ARM200CF in the Electron Microscopy Service (Research Resources Center, UIC). XPS was performed at the Center for Nanoscale Systems at Harvard University. The authors also acknowledge the use and support of the Maryland NanoCenter and its AIMLab.

REFERENCES

- (1) Hansen, T. W.; DeLaRiva, A. T.; Challa, S. R.; Datye, A. K. Sintering of catalytic nanoparticles: particle migration or ostwald ripening? *Acc. Chem. Res.* **2013**, *46*, 1720–1730.
- (2) Banham, D.; Ye, S.; Pei, K.; Ozaki, J.-I.; Kishimoto, T.; Imashiro, Y. A review of the stability and durability of non-precious metal catalysts for the oxygen reduction reaction in proton exchange membrane fuel cells. *J. Power Sources* **2015**, 285, 334–348.
- (3) Zhang, G.; Chenitz, R.; Lefèvre, M.; Sun, S.; Dodelet, J.-P. Is iron involved in the lack of stability of Fe/N/C electrocatalysts used to reduce oxygen at the cathode of PEM fuel cells? *Nano Energy* **2016**, 29, 111–125.
- (4) Kay Lup, A. N.; Abnisa, F.; Wan Daud, W. M. A.; Aroua, M. K. A review on reactivity and stability of heterogeneous metal catalysts for deoxygenation of bio-oil model compounds. *J. Ind. Eng. Chem.* **2017**, *56*, 1–34.
- (5) Carter, J. H.; Liu, X.; He, Q.; Althahban, S.; Nowicka, E.; Freakley, S. J.; Niu, L.; Morgan, D. J.; Li, Y.; Niemantsverdriet, J. W.; Golunski, S.; Kiely, C. J.; Hutchings, G. J. Activation and deactivation of gold/ceria-zirconia in the low-temperature water-gas shift reaction. *Angew. Chem., Int. Ed.* **2017**, *56*, 16037–16041.
- (6) Aydin, C.; Lu, J.; Browning, N. D.; Gates, B. C. A "smart" catalyst: Sinter-resistant supported iridium clusters visualized with electron microscopy. *Angew. Chem., Int. Ed.* **2012**, *51*, 5929–5934.

- (7) Bliem, R.; van der Hoeven, J. E. S.; Hulva, J.; Pavelec, J.; Gamba, O.; de Jongh, P. E.; Schmid, M.; Blaha, P.; Diebold, U.; Parkinson, G. S. Dual role of CO in the stability of subnano Pt clusters at the Fe₃O₄(001) surface. *Proc. Natl. Acad. Sci. U. S. A.* **2016**, *113*, 8921–8926
- (8) Corma, A.; Concepción, P.; Boronat, M.; Sabater, M. J.; Navas, J.; Yacaman, M. J.; Larios, E.; Posadas, A.; López-Quintela, M. A.; Buceta, D.; Mendoza, E.; Guilera, G.; Mayoral, A. Exceptional oxidation activity with size-controlled supported gold clusters of low atomicity. *Nat. Chem.* **2013**, *5*, 775.
- (9) Uzun, A.; Gates, B. C. Real-time characterization of formation and breakup of iridium clusters in highly dealuminated zeolite Y. *Angew. Chem., Int. Ed.* **2008**, 47, 9245–9248.
- (10) Yu, P.; Pemberton, M.; Plasse, P. PtCo/C cathode catalyst for improved durability in PEMFCs. J. Power Sources 2005, 144, 11–20.
- (11) Bing, Y.; Liu, H.; Zhang, L.; Ghosh, D.; Zhang, J. Nanostructured Pt-alloy electrocatalysts for PEM fuel cell oxygen reduction reaction. *Chem. Soc. Rev.* **2010**, *39*, 2184–2202.
- (12) Gewirth, A. A.; Thorum, M. S. Electroreduction of dioxygen for fuel-cell applications: Materials and challenges. *Inorg. Chem.* **2010**, *49*, 3557–3566.
- (13) Ferreira, P. J.; la O', G. J.; Shao-Horn, Y.; Morgan, D.; Makharia, R.; Kocha, S.; Gasteiger, H. A. Instability of Pt/C electrocatalysts in proton exchange membrane fuel cells: A mechanistic investigation. *J. Electrochem. Soc.* **2005**, *152*, A2256–A2271.
- (14) Cheng, N.; Stambula, S.; Wang, D.; Banis, M. N.; Liu, J.; Riese, A.; Xiao, B.; Li, R.; Sham, T.-K.; Liu, L.-M.; Botton, G. A.; Sun, X. Platinum single-atom and cluster catalysis of the hydrogen evolution reaction. *Nat. Commun.* **2016**, *7*, 13638.
- (15) Jang, Y. J.; Jang, J.-W.; Lee, J.; Kim, J. H.; Kumagai, H.; Lee, J.; Minegishi, T.; Kubota, J.; Domen, K.; Lee, J. S. Selective CO production by Au coupled ZnTe/ZnO in the photoelectrochemical CO₂ reduction system. *Energy Environ. Sci.* **2015**, *8*, 3597–3604.
- (16) Morales-Guio, C. G.; Tilley, S. D.; Vrubel, H.; Grätzel, M.; Hu, X. Hydrogen evolution from a copper(I) oxide photocathode coated with an amorphous molybdenum sulphide catalyst. *Nat. Commun.* **2014**, *5*, 3059.
- (17) Munir, A.; Haq, T.u.; Qurashi, A.; Rehman, H.u.; Ul-Hamid, A.; Hussain, I. Ultrasmall Ni/NiO nanoclusters on thiol-functionalized and -exfoliated graphene oxide nanosheets for durable oxygen evolution reaction. ACS Appl. Energy Mater. 2019, 2, 363–371.
- (18) Li, W.; Sheehan, S. W.; He, D.; He, Y.; Yao, X.; Grimm, R. L.; Brudvig, G. W.; Wang, D. Hematite-based solar water splitting in acidic solutions: Functionalization by mono- and multilayers of iridium oxygen-evolution catalysts. *Angew. Chem., Int. Ed.* **2015**, *54*, 11428–11432.
- (19) Liu, L.; Corma, A. Metal catalysts for heterogeneous catalysis: From single atoms to nanoclusters and nanoparticles. *Chem. Rev.* **2018**, *118*, 4981–5079.
- (20) Hang Li, Y.; Xing, J.; Jia Chen, Z.; Li, Z.; Tian, F.; Rong Zheng, L.; Feng Wang, H.; Hu, P.; Jun Zhao, H.; Gui Yang, H. Unidirectional suppression of hydrogen oxidation on oxidized platinum clusters. *Nat. Commun.* **2013**, *4*, 2500.
- (21) Lee, S.; Molina, L. M.; López, M. J.; Alonso, J. A.; Hammer, B.; Lee, B.; Seifert, S.; Winans, R. E.; Elam, J. W.; Pellin, M. J.; Vajda, S. Selective propene epoxidation on immobilized Au_{6–10} clusters: the effect of hydrogen and water on activity and selectivity. *Angew. Chem., Int. Ed.* **2009**, *48*, 1467–1471.
- (22) Jeong, H.; Bae, J.; Han, J. W.; Lee, H. Promoting effects of hydrothermal treatment on the activity and durability of Pd/CeO_2 catalysts for CO oxidation. ACS Catal. 2017, 7, 7097–7105.
- (23) Zhao, Y.; Yan, X.; Yang, K. R.; Cao, S.; Dong, Q.; Thorne, J. E.; Materna, K. L.; Zhu, S.; Pan, X.; Flytzani-Stephanopoulos, M.; Brudvig, G. W.; Batista, V. S.; Wang, D. End-on bound iridium dinuclear heterogeneous catalysts on WO₃ for solar water oxidation. *ACS Cent. Sci.* **2018**, *4*, 1166–1172.
- (24) Zhao, Y.; Yang, K. R.; Wang, Z.; Yan, X.; Cao, S.; Ye, Y.; Dong, Q.; Zhang, X.; Thorne, J. E.; Jin, L.; Materna, K. L.; Trimpalis, A.; Bai,

H.; Fakra, S. C.; Zhong, X.; Wang, P.; Pan, X.; Guo, J.; Flytzani-Stephanopoulos, M.; Brudvig, G. W.; Batista, V. S.; Wang, D. Stable iridium dinuclear heterogeneous catalysts supported on metal-oxide substrate for solar water oxidation. *Proc. Natl. Acad. Sci. U. S. A.* **2018**, 115, 2902–2907.

- (25) Yao, X.; Cheng, Q.; Xie, J.; Dong, Q.; Wang, D. Functionalizing titanium disilicide nanonets with cobalt oxide and palladium for stable Li oxygen battery operations. *ACS Appl. Mater. Interfaces* **2015**, *7*, 21948–21955.
- (26) Sheehan, S. W.; Thomsen, J. M.; Hintermair, U.; Crabtree, R. H.; Brudvig, G. W.; Schmuttenmaer, C. A. A molecular catalyst for water oxidation that binds to metal oxide surfaces. *Nat. Commun.* **2015**, *6*, 6469.
- (27) Xue, T.; Lin, Z.; Chiu, C.-Y.; Li, Y.; Ruan, L.; Wang, G.; Zhao, Z.; Lee, C.; Duan, X.; Huang, Y. Molecular ligand modulation of palladium nanocatalysts for highly efficient and robust heterogeneous oxidation of cyclohexenone to phenol. *Sci. Adv.* **2017**, *3*, No. e1600615.
- (28) Wu, L.; Li, Q.; Wu, C. H.; Zhu, H.; Mendoza-Garcia, A.; Shen, B.; Guo, J.; Sun, S. Stable cobalt nanoparticles and their monolayer array as an efficient electrocatalyst for oxygen evolution reaction. *J. Am. Chem. Soc.* **2015**, *137*, 7071–7074.
- (29) Fan, Z.; Zhang, H. Crystal phase-controlled synthesis, properties and applications of noble metal nanomaterials. *Chem. Soc. Rev.* **2016**, 45, 63–82.
- (30) Sankar, M.; Dimitratos, N.; Miedziak, P. J.; Wells, P. P.; Kiely, C. J.; Hutchings, G. J. Designing bimetallic catalysts for a green and sustainable future. *Chem. Soc. Rev.* **2012**, *41*, 8099–8139.
- (31) Gilroy, K. D.; Ruditskiy, A.; Peng, H.-C.; Qin, D.; Xia, Y. Bimetallic nanocrystals: Syntheses, properties, and applications. *Chem. Rev.* **2016**, *116*, 10414–10472.
- (32) Buck, M. R.; Bondi, J. F.; Schaak, R. E. A total-synthesis framework for the construction of high-order colloidal hybrid nanoparticles. *Nat. Chem.* **2012**, *4*, 37.
- (33) Kwon, S. G.; Krylova, G.; Phillips, P. J.; Klie, R. F.; Chattopadhyay, S.; Shibata, T.; Bunel, E. E.; Liu, Y.; Prakapenka, V. B.; Lee, B.; Shevchenko, E. V. Heterogeneous nucleation and shape transformation of multicomponent metallic nanostructures. *Nat. Mater.* **2015**, *14*, 215.
- (34) Ferrando, R.; Jellinek, J.; Johnston, R. L. Nanoalloys: From theory to applications of alloy clusters and nanoparticles. *Chem. Rev.* **2008**, *108*, 845–910.
- (35) Zhang, C.; Oliaee, S. N.; Hwang, S. Y.; Kong, X.; Peng, Z. A generic wet impregnation method for preparing substrate-supported platinum group metal and alloy nanoparticles with controlled particle morphology. *Nano Lett.* **2016**, *16*, 164–169.
- (36) Lonergan, W. W.; Vlachos, D. G.; Chen, J. G. Correlating extent of Pt-Ni bond formation with low-temperature hydrogenation of benzene and 1,3-butadiene over supported Pt/Ni bimetallic catalysts. *J. Catal.* **2010**, *271*, 239–250.
- (37) Alayoglu, S.; Nilekar, A. U.; Mavrikakis, M.; Eichhorn, B. Ru-Pt core-shell nanoparticles for preferential oxidation of carbon monoxide in hydrogen. *Nat. Mater.* **2008**, *7*, 333.
- (38) Buck, M. R.; Schaak, R. E. Emerging strategies for the total synthesis of inorganic nanostructures. *Angew. Chem., Int. Ed.* **2013**, *52*, 6154–6178.
- (39) Chen, P.-C.; Liu, X.; Hedrick, J. L.; Xie, Z.; Wang, S.; Lin, Q.-Y.; Hersam, M. C.; Dravid, V. P.; Mirkin, C. A. Polyelemental nanoparticle libraries. *Science* **2016**, *352*, 1565–1569.
- (40) Chen, P.-C.; Liu, G.; Zhou, Y.; Brown, K. A.; Chernyak, N.; Hedrick, J. L.; He, S.; Xie, Z.; Lin, Q.-Y.; Dravid, V. P.; O'Neill-Slawecki, S. A.; Mirkin, C. A. Tip-directed synthesis of multimetallic nanoparticles. *J. Am. Chem. Soc.* **2015**, *137*, 9167–9173.
- (41) Bruce, P. G.; Freunberger, S. A.; Hardwick, L. J.; Tarascon, J.-M. Li- O_2 and Li-S batteries with high energy storage. *Nat. Mater.* **2012**, *11*, 19.
- (42) Lu, Y. C.; Gallant, B. M.; Kwabi, D. G.; Harding, J. R.; Mitchell, R. R.; Whittingham, M. S.; Shao-Horn, Y. Lithium-oxygen batteries:

Bridging mechanistic understanding and battery performance. *Energy Environ. Sci.* **2013**, *6*, 750–768.

- (43) Girishkumar, G.; McCloskey, B.; Luntz, A. C.; Swanson, S.; Wilcke, W. Lithium-air battery: Promise and challenges. *J. Phys. Chem. Lett.* **2010**, *1*, 2193–2203.
- (44) Lu, J.; Li, L.; Park, J.-B.; Sun, Y.-K.; Wu, F.; Amine, K. Aprotic and aqueous Li-O₂ batteries. *Chem. Rev.* **2014**, *114*, 5611–5640.
- (45) Wang, Z.-L.; Xu, D.; Xu, J.-J.; Zhang, X.-B. Oxygen electrocatalysts in metal-air batteries: From aqueous to nonaqueous electrolytes. *Chem. Soc. Rev.* **2014**, 43, 7746–7786.
- (46) Chang, Z.; Xu, J.; Zhang, X. Recent progress in electrocatalyst for Li-O₂ batteries. *Adv. Energy Mater.* **2017**, *7*, 1700875.
- (47) Dong, Q.; Wang, D. Catalysts in metal-air batteries. MRS Commun. 2018, 8, 372-386.
- (48) Yao, X.; Dong, Q.; Cheng, Q.; Wang, D. Why do lithium-oxygen batteries fail: Parasitic chemical reactions and their synergistic effect. *Angew. Chem., Int. Ed.* **2016**, *55*, 11344–11353.
- (49) Luntz, A. C.; McCloskey, B. D. Nonaqueous Li-Air batteries: A status report. *Chem. Rev.* **2014**, *114*, 11721–11750.
- (50) Feng, N.; He, P.; Zhou, H. Critical challenges in rechargeable aprotic Li-O, batteries. *Adv. Energy Mater.* **2016**, *6*, 1502303.
- (51) McCloskey, B. D.; Addison, D. A viewpoint on heterogeneous electrocatalysis and redox mediation in nonaqueous Li-O₂ batteries. *ACS Catal.* **2017**, *7*, 772–778.
- (52) Li, L.; Chai, S.-H.; Dai, S.; Manthiram, A. Advanced hybrid Liair batteries with high-performance mesoporous nanocatalysts. *Energy Environ. Sci.* **2014**, *7*, 2630–2636.
- (53) Yao, Y.; Huang, Z.; Xie, P.; Lacey, S. D.; Jacob, R. J.; Xie, H.; Chen, F.; Nie, A.; Pu, T.; Rehwoldt, M.; Yu, D.; Zachariah, M. R.; Wang, C.; Shahbazian-Yassar, R.; Li, J.; Hu, L. Carbothermal shock synthesis of high-entropy-alloy nanoparticles. *Science* **2018**, 359, 1489—1494.
- (54) Ottakam Thotiyl, M. M.; Freunberger, S. A.; Peng, Z.; Bruce, P. G. The carbon electrode in nonaqueous Li-O₂ cells. *J. Am. Chem. Soc.* **2013**, 135, 494–500.
- (55) Lin, Y.; Moitoso, B.; Martinez-Martinez, C.; Walsh, E. D.; Lacey, S. D.; Kim, J.-W.; Dai, L.; Hu, L.; Connell, J. W. Ultrahigh-capacity lithium-oxygen batteries enabled by dry-pressed holey graphene air cathodes. *Nano Lett.* **2017**, *17*, 3252–3260.
- (56) Luo, J.; Yao, X.; Yang, L.; Han, Y.; Chen, L.; Geng, X.; Vattipalli, V.; Dong, Q.; Fan, W.; Wang, D.; et al. Free-standing porous carbon electrodes derived from wood for high-performance Li-O₂ battery applications. *Nano Res.* **2017**, *10*, 4318–4326.
- (57) Chang, Z.-w.; Xu, J.-j.; Liu, Q.-C.; Li, L.; Zhang, X.-b. Recent progress on stability enhancement for cathode in rechargeable non-aqueous lithium-oxygen battery. *Adv. Energy Mater.* **2015**, *5*, 1500633.
- (58) Yang, Y.; Chiang, K.; Burke, N. Porous carbon-supported catalysts for energy and environmental applications: A short review. *Catal. Today* **2011**, *178*, 197–205.
- (59) Xie, J.; Yao, X.; Cheng, Q.; Madden, I. P.; Dornath, P.; Chang, C.-C.; Fan, W.; Wang, D. Three dimensionally ordered mesoporous carbon as a stable, high-performance Li-O₂ battery cathode. *Angew. Chem., Int. Ed.* **2015**, 54, 4299–4303.
- (60) Guo, Z.; Zhou, D.; Dong, X.; Qiu, Z.; Wang, Y.; Xia, Y. Ordered hierarchical mesoporous/macroporous carbon: A high-performance catalyst for rechargeable Li-O₂ batteries. *Adv. Mater.* **2013**, 25, 5668–5672.
- (61) Dornath, P.; Ruzycky, S.; Pang, S.; He, L.; Dauenhauer, P.; Fan, W. Adsorption-enhanced hydrolysis of glucan oligomers into glucose over sulfonated three-dimensionally ordered mesoporous carbon catalysts. *Green Chem.* **2016**, *18*, 6637–6647.
- (62) Liao, K.; Zhang, T.; Wang, Y.; Li, F.; Jian, Z.; Yu, H.; Zhou, H. Nanoporous Ru as a carbon- and binder-free cathode for Li-O₂ batteries. *ChemSusChem* **2015**, *8*, 1429–1434.
- (63) Xie, J.; Yao, X.; Madden, I. P.; Jiang, D.-E.; Chou, L.-Y.; Tsung, C.-K.; Wang, D. Selective deposition of Ru nanoparticles on TiSi₂ nanonet and itsutilization for Li₂O₂ formation and decomposition. *J. Am. Chem. Soc.* **2014**, *136*, 8903–8906.

(64) Li, F.; Tang, D.-M.; Chen, Y.; Golberg, D.; Kitaura, H.; Zhang, T.; Yamada, A.; Zhou, H. Ru/ITO: A carbon-free cathode for nonaqueous Li-O₂ battery. *Nano Lett.* **2013**, 13, 4702–4707.

- (65) Li, F.; Chen, Y.; Tang, D.-M.; Jian, Z.; Liu, C.; Golberg, D.; Yamada, A.; Zhou, H. Performance-improved Li-O₂ battery with Ru nanoparticles supported on binder-free multi-walled carbon nanotube paper as cathode. *Energy Environ. Sci.* **2014**, *7*, 1648–1652.
- (66) Lu, J.; Jung Lee, Y.; Luo, X.; Chun Lau, K.; Asadi, M.; Wang, H.-H.; Brombosz, S.; Wen, J.; Zhai, D.; Chen, Z.; Miller, D. J.; Sub Jeong, Y.; Park, J.-B.; Zak Fang, Z.; Kumar, B.; Salehi-Khojin, A.; Sun, Y.-K.; Curtiss, L. A.; Amine, K. A lithium—oxygen battery based on lithium superoxide. *Nature* **2016**, *529*, 377—382.
- (67) Papp, J. K.; Forster, J. D.; Burke, C. M.; Kim, H. W.; Luntz, A. C.; Shelby, R. M.; Urban, J. J.; McCloskey, B. D. Poly(vinylidene fluoride) (PVDF) binder degradation in Li-O₂ batteries: A consideration for the characterization of lithium superoxide. *J. Phys. Chem. Lett.* **2017**, *8*, 1169–1174.
- (68) Wang, D.; Li, Y. Bimetallic nanocrystals: Liquid-phase synthesis and catalytic applications. *Adv. Mater.* **2011**, 23, 1044–1060.
- (69) Fan, W.; Snyder, M. A.; Kumar, S.; Lee, P.-S.; Yoo, W. C.; McCormick, A. V.; Lee Penn, R.; Stein, A.; Tsapatsis, M. Hierarchical nanofabrication of microporous crystals with ordered mesoporosity. *Nat. Mater.* **2008**, *7*, 984.
- (70) Jung, H.-G.; Jeong, Y. S.; Park, J.-B.; Sun, Y.-K.; Scrosati, B.; Lee, Y. J. Ruthenium-based electrocatalysts supported on reduced graphene oxide for lithium-air batteries. *ACS Nano* **2013**, *7*, 3532–3539.
- (71) Aurbach, D.; McCloskey, B. D.; Nazar, L. F.; Bruce, P. G. Advances in understanding mechanisms underpinning lithium—air batteries. *Nat. Energy* **2016**, *1*, 16128.
- (72) Suo, L.; Borodin, O.; Gao, T.; Olguin, M.; Ho, J.; Fan, X.; Luo, C.; Wang, C.; Xu, K. Water-in-salt" electrolyte enables high-voltage aqueous lithium-ion chemistries. *Science* **2015**, *350*, 938–943.
- (73) Dong, Q.; Yao, X.; Zhao, Y.; Qi, M.; Zhang, X.; Sun, H.; He, Y.; Wang, D. Cathodically stable Li-O₂ battery operations using water-insalt electrolyte. *Chem* **2018**, *4*, 1345–1358.